ACS APPLIED NANO MATERIALS

www.acsanm.org Article

Nonstoichiometric Copper Sulfide Nanostructures at the Brass–Rubber Interface: Implications for Rubber Vulcanization Temperature in the Tire Industry

M. P. Kannan, Anirban Som, Tripti Ahuja, Vidhya Subramanian, A. Sreekumaran Nair,* and Thalappil Pradeep*

Cite This: *ACS Appl. Nano Mater.* 2020, 3, 7685–7694 Read Online

ACCESS | Metrics & More | Article Recommendations | Supporting Information

ABSTRACT: Brass (which is an alloy of copper and zinc)-coated steel cords (BCSCs) in the form of belts are embedded in a rubber compound in radial tires (beneath the tread) to give stability and strength to the tread region of the tires. The life of the tires also depends on the strength and durability of the bond between the BCSCs and rubber. During the vulcanization process with sulfur, a series of sulfide and oxide nanostructures of copper and zinc are formed at the brass–rubber interface. These nanostructures have a dendritic morphology that can reinforce rubber primarily through mechanical interlocking created through the flow of rubber chains into the dendritic cavities followed by formation of cross-links between rubber chains during vulcanization. The strength and durability of the bonding depend on a number of parameters such as rubber compound formulation, vulcanization temperature (VT) and time, nanostructure thickness (height), and chemical composition of the nanostructures (the so-called adhesion interface). A few methods have been stated in the literature for assessing the chemical composition and thickness of the adhesion interface. However, simple, reliable, and newer methodologies are needed for a better understanding of the same. This paper details a new approach called the "brass mesh experiment" to assess the thickness of the adhesion interface formed under particular vulcanization conditions using microscopy. Raman imaging and spectroscopy were employed to determine the chemical composition of the interface with complementary data from X-ray photoelectron spectroscopy and X-ray diffraction. Using the methodologies, VT optimization was done for a tire compound formulation, and this was verified by the generally accepted pull-out force method. We believe that the methodologies outlined in this paper can trigger further research for a better understanding of the adhesion interface in radial tires.

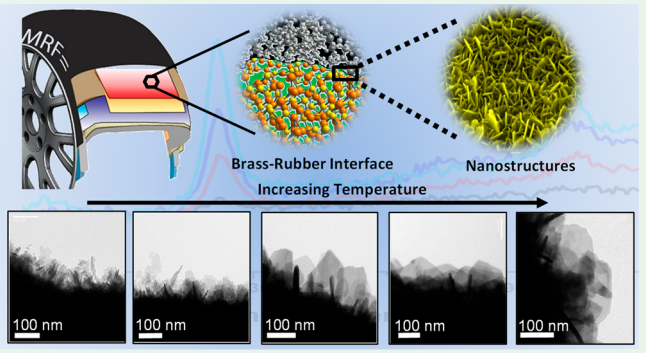

KEYWORDS: *brass–rubber interface, nonstoichiometric copper sulfide, Raman imaging, adhesion, vulcanization, interfacial nanostructures*

INTRODUCTION

Radial design, a game changer in tire technology, revolutionized the world of tires for its excellent combination of low fuel consumption, softer ride, and long service life.[1,2] On road, the ply region of the radial tire (RT) experiences maximum stress and is prone to deformation upon prolonged usage.[3] This fundamental problem necessitates the requirement of extensive use of brass-coated steel cords (BCSCs) as reinforcing materials embedded in the ply region perpendicular to the direction of its movement on the road, thereby enhancing the durability of tires.[2,4] The brass layer is deposited on steel wires through electrolysis in a cyanide solution. Treatment processes like current density, pH, copper (Cu) to zinc (Zn) ratio, and temperature play an important role in adjusting the composition of the brass. Finally, a heat treatment (650 °F) is done to improve coating continuity and surface composition. The surface composition of BCSC in contact with rubber (before vulcanization) is depicted in Figure 1.

Under normal conditions, the ply rubber compound (a terminology used in the tire literature, referring to a mixture of natural rubber, carbon black, and sulfur) and BCSC do not adhere to each other. This is when the vulcanization method comes into play. In general, various vulcanization methods are followed to prepare a metal–rubber composite like compres-

Received: May 12, 2020
Accepted: July 20, 2020
Published: July 20, 2020

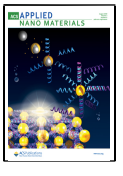

https://dx.doi.org/10.1021/acsanm.0c01298
ACS Appl. Nano Mater. 2020, 3, 7685–7694

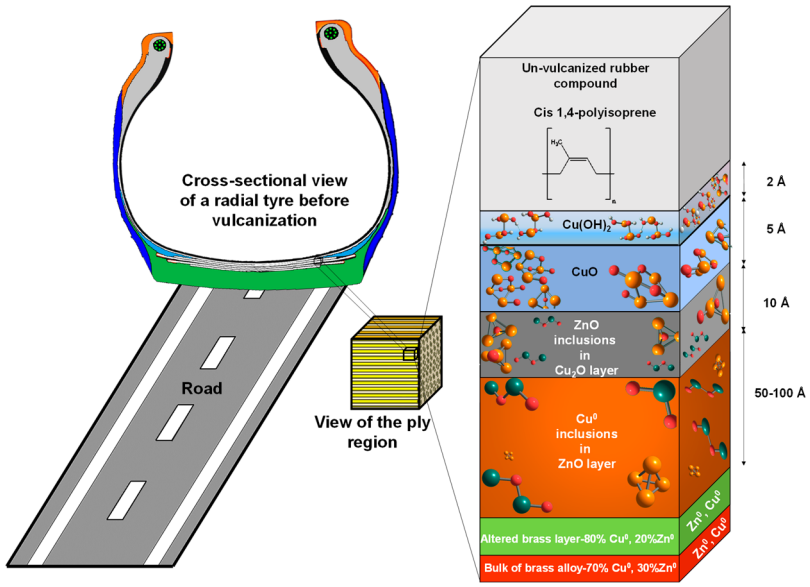

Figure 1. Schematic representation of the brass−rubber interface before vulcanization. The species and thickness mentioned are not to scale.

sion and injection molding.[5,6] The most predominant happens to be the compression molding technique that uses sliced pieces of rubber compound matching the size of a metal mold cavity.[7] This assembly is layered with cut BCSC and another rubber compound creating a sandwich-like structure. The mold is preheated at different temperatures based on the requirement. Later, the vulcanization of the sandwiched BCSC structure is performed in the mold with pressures higher than 3.5 MPa and is maintained constant throughout the molding cycle. During vulcanization, both the systems adhere by the formation of an interface with a dendritic morphology composed of copper(II) sulfide (CuS), copper(I) sulfide (Cu_2S), nonstoichiometric copper sulfides ($Cu_{2-x}S$), ZnO, and zinc(II) sulfide (ZnS). At the early stages of vulcanization, the degree of S−rubber cross-linking is small, and hence the rubber will be in a viscous state. As vulcanization proceeds, the rubber starts to flow into the dendrites having a mixture of CuS, Cu_2S, $Cu_{2-x}S$, ZnO, and ZnS (wetting process) and interlocks rigidly, leading to robust interfacial adhesion.[8−10] The strength of the interface formed in the ply region is the lifeline of RTs, and it is a skill to engineer the interface to achieve maximum interfacial strength which is determined by the optimum growth of the interfacial nanostructures.[11−14]

From several microscopic and spectroscopic studies such as scanning electron microscopy (SEM), cross-sectional transmission electron microscopy (TEM), X-ray photoelectron spectroscopy (XPS) depth profiling, Raman spectroscopy, time-of-flight secondary ion mass spectrometry (TOF-SIMS), and X-ray diffraction (XRD), it has been inferred that various factors such as interface thickness, morphology, crystal phase, and chemical composition at the interface play a significant role in enhancing adhesion between brass and rubber.[15−28] However, these techniques have their own limitations and inadequacies.[13,16,19,20,26,27,29,30] Some limitations include a cumbersome preparation process (sectioning and ion polishing) for TEM and damage of the sample due to the use of argon ion (Ar^+) sputtering (for XPS), and therefore a new methodology for the measurement of interfacial characteristics is necessary.[12,13]

Several issues apparent in the literature are presented below. SEM suggested that copper sulfide nanostructures were formed only in some regions of the vulcanized BCSCs, which made information about interfacial bonding inconclusive.[30] Until 1977, tire chemists have dealt with the identification of only CuS and Cu_2S crystalline phases in the adhesion interface. Subsequent investigations using grazing incidence XRD (GIXRD) have shown that $Cu_{1.8}S$ is also formed along with CuS and Cu_2S.[31] XPS studies, since 1980, helped in understanding the interfacial chemical composition. Researchers have established the relative atomic percentages of elements at the interface during vulcanization. However, a fundamental knowledge gap still exists on the chemical states of elements at different VTs.[26] Raman spectroscopy and imaging tools were relatively unexplored in finding the composition of the interface, except for a report on a model system involving ionic liquid and S.[32] Previous work in understanding the role of VT on the brass−rubber interface is insufficient.[15] There is still considerable uncertainty concerning the morphology and interface thickness as a function of VT.

Despite the vast amount of literature on the subject, a reliable methodology to assess the interfacial thickness and its chemical composition is still nonexistent. Here, we present a novel method for measuring the interface thickness by a "brass mesh experiment" using transmission electron microscopy. The methodology helped us to understand the evolution of morphology of the copper sulfide nanostructures at the interface with an increase in VT and find the different crystalline phases formed at the interface. The study also presents, for the first time, the usefulness of Raman imaging to see the spatial distribution of chemical species at the interface, specifically the distribution of sulfides and oxides of copper and zinc. This paper also features a comprehensive investigation using complementary techniques such as FESEM, XRD, and XPS. Because the vulcanization of the rubber compound along with BCSC/mesh was performed at the pressure and time used in actual RTs, the results reported here are closer to reality, providing new insights for rubber technologists.

https://dx.doi.org/10.1021/acsanm.0c01298
ACS Appl. Nano Mater. 2020, 3, 7685−7694

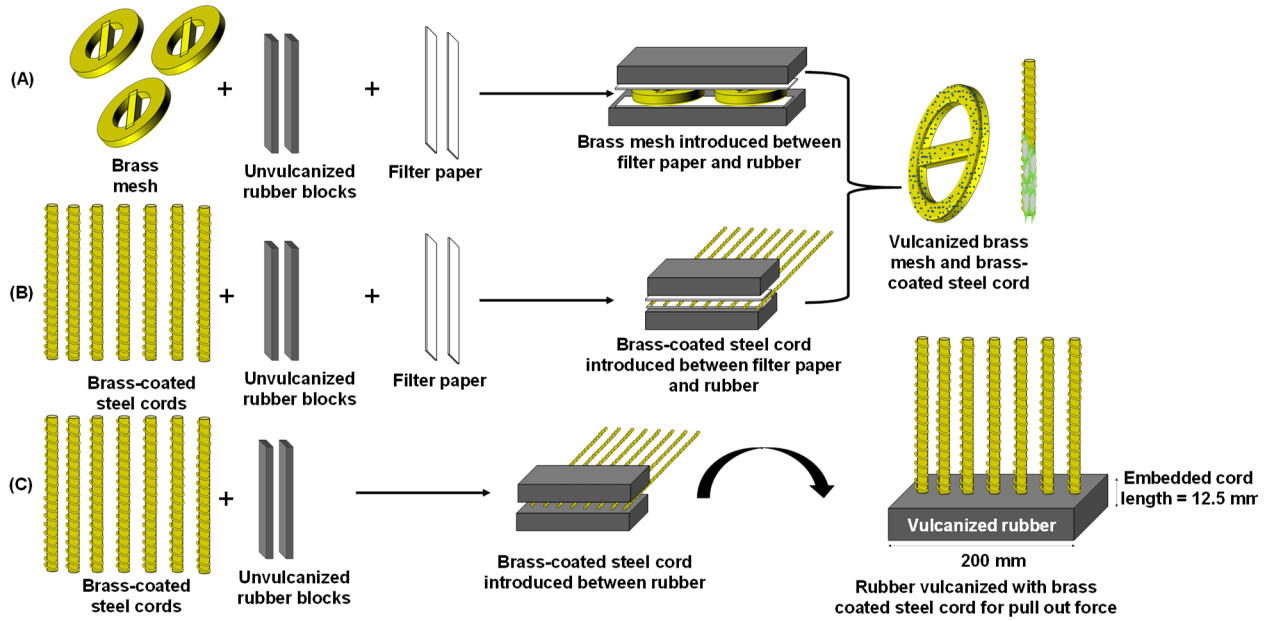

Figure 2. Schematic showing vulcanization procedure used for sample preparation. (A, B) Vulcanization of brass mesh and BCSC using the filter paper method. (C) Vulcanization of rubber block with BCSC for performing the POF.

MATERIALS AND METHODS

Rubber Compound Preparation. The preparation of the rubber compound proceeds in two stages. Raw materials such as natural rubber, fillers, plasticizers, activators, adhesion promoters, S (in the form of S_8), *N*-dicyclohexylbenzothiazole-2-sulfenamide (DCBS), and methylene donor and acceptor were mixed in a Kobelco lab Banbury (1.8 L capacity) in stage 1. Subsequently, S and DCBS were added into the rubber mixer in stage 2. The prepared rubber compound was then vulcanized along with BCSC by using the filter paper method.[29] The raw materials were procured from bulk manufacturers.

Interfacial Thickness Measurement Using Brass Mesh Experiment. A brass foil having 0.3 mm thickness with an equivalent composition to that of industrial BCSC was purchased from Krishna Copper Private Limited (Gujarat, India). The foil was then cut to a 3.05 mm diameter with a YAG laser (Nd:YAG Laser Tech., India), operating at a power of 800 W. Figure S1 shows a schematic of the prepared brass mesh which was then used in the filter paper method.

Sample Preparation. BCSCs having a brass composition of 70% Cu and 30% Zn were used in the present investigation. The filter paper method was used to understand the growth of nanostructures on brass surfaces during the process of vulcanization. It creates a clean modified metal surface without the rubber covering it and is therefore useful for spectroscopic and microscopic investigations. Whatman grade 42 filter paper of 12.5 cm diameter and pore size of 2.5 μm manufactured by GE Healthcare Life Sciences was procured from Modern Scientific, India. The rubber compound was kept on either side of the two filter papers, as shown in Figure 2A,B, and the regions between the filter papers were sandwiched with the brass mesh (for TEM) and steel cord (for SEM, XPS, XRD, and Raman). Filter papers prevent the polymer and carbon black from interacting directly with the brass surfaces; however, they will allow S, accelerator, and metal ions from the vulcanizing mix to pass through and react with the brass surfaces.[29] This sandwiched assembly was then vulcanized at different temperatures. Post-vulcanization, the rubber was cut open to remove the reacted BCSC and the brass mesh. The samples were hermetically sealed in a N_2 atmosphere before analyses.

Characterization. The nanostructures grown on the BCSC and the brass mesh were analyzed by using different characterization techniques. The morphology of the nanostructures was observed with a NanoSEM 600 field-emission scanning electron microscope (FESEM) at 10 kV. The crystallinity of the nanostructures was studied by using XRD with a Bruker D8 discovery diffractometer using Cu Kα radiation (wavelength = 1.54 Å) between 10° and 80° (2θ) with a step size of 0.1°. XRD results were analyzed by using X'Pert HighScore software. JEOL TEM was used at an electron accelerating voltage of 200 kV to image the brass mesh. ImageJ software was used to calculate the thickness of interface formed on the brass mesh. Data from 20 such TEM measurements were taken for the calculation of the average interface thickness. To understand the chemical state of the species formed at the interface, XPS was performed by using an ESCA probe TPD spectrometer of Omicron Nanotechnology with a polychromatic Al Kα ($h\upsilon$ = 1486.6 eV) X-ray source. The binding energy of all the elements was calibrated with respect to C 1s at 284.8 eV. Finally, in an attempt to understand the distribution of sulfides and oxides of Cu and Zn along vulcanized BCSC, a CRM Alpha 300 S AFM-Raman spectrometer of WiTec GmbH (Germany, 633 nm laser excitation) was used to perform Raman spectroscopy and Raman imaging.

Preparation of Metal−Rubber Composite. The compression molding technique was used to prepare a metal−rubber composite having dimensions of 200 mm × 12.5 mm (Figure 2C).[5,6] This procedure starts with making a thin sheet of the rubber compound and cutting it into pieces that fit into a metal mold cavity.[7] BCSCs were cut carefully and placed over the rubber compound in the mold as shown in Figure 2C. To this rubber compound, one more layer of the rubber block was assembled. The mold was then preheated to different temperatures (130−170 °C) based on the requirement. Later the top mold was placed over the bottom half and then clamped by a steel bar to stop the BCSC from moving during molding. Vulcanization of BCSCs assembled between the rubber compounds was performed in the mold at different temperatures with a pressure of more than 3.5 MPa on the mold surface. The pressure helped the rubber to be in contact with the whole of the mold area. Temperature and pressure were maintained constant throughout the molding cycle. Post-vulcanization, the compression molding process produces rubber flashes that were removed. After vulcanization, the blocks were preserved at room temperature for 16 h before testing.

Pull-Out Force (POF) Experiment. The POF test method measures the force necessary to pull out the vulcanized BCSCs out of rubber.[33] A POF experiment begins with preparation of the sample specimen. The steel cords along with the rubber were vulcanized according to ASTM D2229. The POF measurement was performed at 24 ± 2 °C by using the Instron 3300 series universal testing system. Figure S2 shows a schematic of the POF measurement system. The equipment consists of a lower fixture to place the vulcanized rubber

https://dx.doi.org/10.1021/acsanm.0c01298
ACS Appl. Nano Mater. 2020, 3, 7685−7694

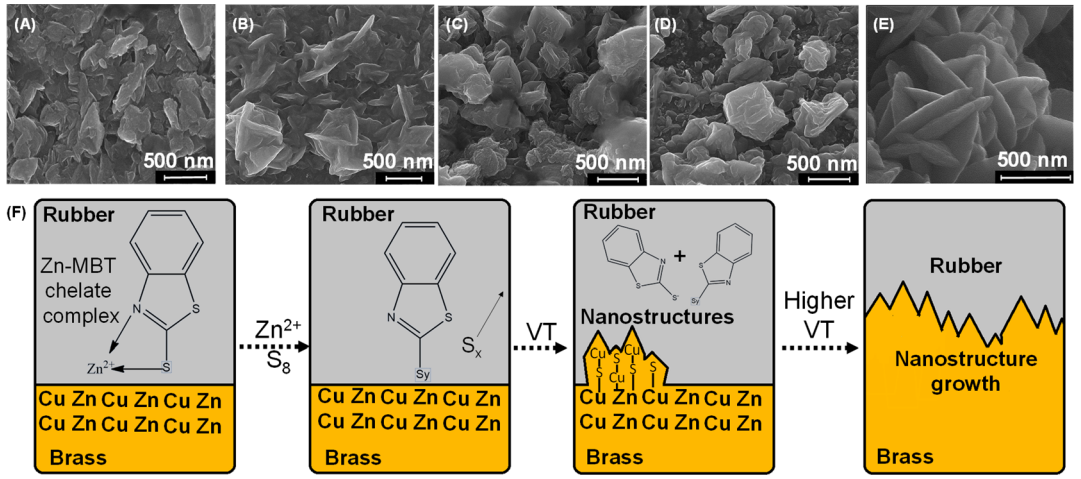

Figure 3. Field-emission scanning electron micrographs of the nanostructures formed at various VTs: (A) 130, (B) 140, (C) 150, (D) 160, and (E) 170 °C. (F) Schematic showing the mechanism of growth of nanostructures at the interface. S_x and S_y in the mechanism represent S_1 to S_8.

block and a clamp to hold BCSCs (Figure S2A). The vulcanized rubber block was pushed to the lower fixture of the equipment and made sure that the sample could be moved inside the fixture without damaging the specimen (Figure S2B). The steel wire was then clamped to the bracket and pulled (Figure S2C,D). The steel cords pulled out of the rubber block were preserved to examine the amount of rubber coverage on the steel cords.

RESULTS AND DISCUSSION

Morphology of Nanostructures Formed on the BCSC Using FESEM and EDS. Figure 3A–E presents the formation of nanostructures as a function of VT (from 130 to 170 °C). The nanostructures formed at the interface mechanically interlocks with the rubber, and this results in adhesion. It is quite apparent from the SEM images that there is a change in the interfacial morphology and surface roughness as a function of VT. The formation of flaky nanostructures on the surface was noticeable at 130 °C. A further increase in temperature to 140 °C showed the growth of the flaky nanostructures. The morphology of the nanostructures was changed from flaky to nanopillar-like structures with increase in VT (from 130 to 140 °C). At VTs higher than 150 °C (i.e., at 160 and 170 °C, respectively), further growth of the nanostructures was observed. Overall, these observations indicated that the morphology of the nanostructures in the brass–rubber interface can be controlled with VT. During vulcanization, continuous diffusion of active sulfurating species (from rubber) to brass surface results in interfacial growth. At higher VTs, the concentration of active sulfurating species at the interface is high, and this leads to the growth of larger and thicker nanostructures.[15] Additionally, we have obtained optical microscopic images (Figure S3) of the BCSC at different VTs to verify the consistency of the vulcanization.

Energy-dispersive X-ray spectroscopy (EDS) was used to get the concentration (wt %) of different elements at the interface. Figure S4 shows the EDS spectra of the vulcanized steel cords at temperatures between 130 and 170 °C. Raster scanning at more than three places of the vulcanized steel cord revealed the presence of significant amounts of Cu, Zn, Fe, S, and O. There were significant differences in the concentrations of Cu and Zn (could have originated from CuS, $Cu_{2-x}S$, Cu_2S, ZnS, and ZnO) with increase in VT. However, a clear trend of increase in concentrations of Fe and O was noticeable between 130 and 170 °C. At higher VTs, increase in intensities of S (Figure S4) indicated the increased formation of the sulfides of Cu and Zn. The most surprising aspect of the EDS result is the absence of cobalt (Co) precursor that was added to the rubber compound for enhancing interfacial adhesion, suggesting that the concentration of Co could be below the detection limit of EDS. As per Table S1, higher VT also promotes a higher rubber–rubber cross-link (cross-link density) through S.[34] Additionally, VT affects the physical properties such as modulus, tensile strength, and elongation at break (EB) of the rubber. The 10%, 100%, and 300% modulus signify the tensile strength of the rubber at 10%, 100%, and 300% elongation of rubber compound at different VTs.[35] From Figure S5, it is seen that 10%, 100%, and 300% modulus of rubber decrease with increased VT, implying that the rubber has become harder and breaks at high VT.[15] The EB of the rubber compound decreases with an increase in VT, implying that the rubber vulcanized at higher VTs fractures easily.

Mechanism of Nanostructure Growth. Figure 3F depicts the growth of metal sulfide nanostructures at the interface that could be explained through a series of steps highlighting the formation of a rubber accelerator intermediate (2-mercaptobenzothiazole (MBT), 2,2′-dithiobenzothiazole (MBTS), zinc–MBTS (ZMBTS), and active sulfurating complex). The characterization of these chemical structures has been done by using TOF-SIMS.[8] The nanostructure growth begins with the partial dissolution of ZnO on the surface of BCSC by a vulcanization promoter, stearic acid, present in the rubber compound ($ZnO + 2C_{17}H_{35}COOH \rightarrow Zn(OOCC_{17}H_{35})_2 + H_2O$).[12] This reaction exposes pure brass, thereby increasing its surface activity. At the same time, the vulcanization accelerator, DCBS, present in the rubber compound dissociates into MBT and MBTS.[36] In the next stage, Zn^{2+} forms a chelate with MBT and attaches it to the N and S sites to form ZMBTS. Simultaneously, the S_7—S^- (S ion) is formed from S_8, which then reacts with ZMBTS to form dibenzothiazole polysulfide (DBTP or active sulfurating complex). In addition, DBTP reacts with the surface of brass, forming a metal–S–accelerator bond (Cu/Zn–S–Acc). At elevated vulcanization temperatures, Cu/Zn–S–Acc bonds dissociate to form Cu/Zn sulfides and a polysulfide accelerator intermediate (S_{x-1}–Acc where $x = 8$). The sulfidation reaction happening during vulcanization is a diffusion-driven process, where constant diffusion of Cu to the surface of brass occurs,

https://dx.doi.org/10.1021/acsanm.0c01298
ACS Appl. Nano Mater. 2020, 3, 7685–7694

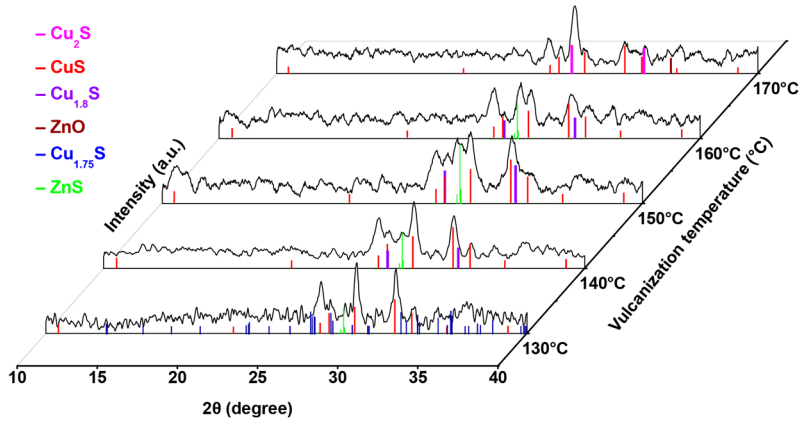

Figure 4. XRD patterns of the vulcanized BCSC at different VTs.

thus thickening the interface. Diffused Cu further reacts with accelerator moieties to form $Cu_{2-x}S$.[13] Consequently, the growth of nanostructures continues to happen due to the buildup of the active sulfurating complex near the brass surface. $Cu_{2-x}S$ consists of cationic vacancies through which Cu^+ ions diffuse to the surface.[12] At higher VTs, it is expected to have more active sulfurating complex on the brass surface, leading to the growth of thicker and larger nanostructures.[15]

Crystallinity of the Adhesion Interface Using XRD. A crystalline interface does not provide enough adhesion with rubber, and it fails quickly. It is also well known that higher VTs contribute to the conversion of an amorphous interface to a crystalline interface, leading to a brittle adhesion layer between BCSC and rubber. Hence, we performed XRD studies to identify different crystalline phases formed at the interface at different VTs. Figure S6 portrays the XRD pattern of unvulcanized BCSC. Before vulcanization, the most prominent peaks correspond to those of brass. Figure 4 illustrates the XRD patterns of the vulcanized steel cords as a function of temperature. It has been reported in the literature that recognition of $Cu_{2-x}S$ crystallographic phases is difficult as it exists in diverse crystal structures and compositions.[37−39] However, the coexistence of multiple phases of $Cu_{2-x}S$ (CuS, anilite ($Cu_{1.75}S$), digenite ($Cu_{1.8}S$), and chalcocite (Cu_2S)) has been observed in our present work along with other chemical species like ZnS and ZnO. The proportions in which these chemical species ($Cu_{2-x}S$, Cu_2S, CuS, ZnS, and ZnO) get formed during vulcanization is important in interfacial adhesion.[40,41] At 130 °C, the diffraction patterns of the steel cords matched with those of $Cu_{1.75}S$ (ICSD no. 16011), CuS (ICSD no. 26968), and ZnS (ICSD no. 107176). Formations of CuS and $Cu_{1.8}S$ (ICSD no. 57213) along with ZnS were noted at 140 °C. The composition remained almost the same until 160 °C while CuS, Cu_2S (ICSD no. 159435), and ZnO (ICSD no. 163382) were present at 170 °C. Vulcanization at a lower temperature leads to the formation of CuS, $Cu_{1.75}S$, $Cu_{1.8}S$, and ZnS at the brass−rubber interface. However, this was overtaken by the formation of CuS, Cu_2S, and ZnO at 170 °C (Table 1). An interface comprising the right ratios of CuS, $Cu_{1.8}S$, and ZnS formed at a VT of 140 °C must be the probable reason for increased POF. These findings help us to understand that 140 °C serves as the optimum VT for the formation of the right adhesion interface with the present rubber formulation.

Measurement of Interfacial Thickness and Understanding the Formation of the Multiphase Junction by TEM. In this section, we demonstrate a new methodology of estimating the thickness of the brass−rubber interface through the brass-mesh experiment. The SEM images showed that temperature is a crucial parameter for the growth of the nanostructures at the interface. A new approach was therefore adopted in the present work which helps us to quantify the interfacial thickness at various VTs. This involved the *in situ* growth of the interface on the brass mesh as explained before. Upon varying the VT, the average interfacial thickness was tuned between 50 and 190 nm, as illustrated in Figures 5A−E and 5F. The average interfacial thickness was around 100 nm at 140 °C and increased to 120 nm at 150 °C. A further increase in temperature to 160 and 170 °C resulted in the formation of heightened hexagon-shaped structures with an average thickness of 168 and 189 nm, respectively. It is encouraging to compare the interfacial thickness to the values of POF (a generally accepted means to test the interfacial strength). Comparing Figure 5A−E with Figure 5F−H, we intrepret that the adhesion is determined by the interface thickness.

Table 1. Crystalline Composition of the Brass−Rubber Interface at Different VTs

S. no.	vulcanization temp (°C)	crystalline composition at the brass−rubber interface
1	130	CuS, $Cu_{1.75}S$, and ZnS
2	140−160	CuS, $Cu_{1.8}S$, and ZnS
3	170	CuS, Cu_2S, and ZnO

The interfacial structures grow in size from ∼92 to ∼189 nm as the VT is increased from 130 to 170 °C. However, the POF displayed a different trend, first increasing with an increase of VT from 130 to 140 °C and subsequently reducing with a further increase of VT from 150 to 170 °C. This is because the growth of the interfacial nanostructures reaches an optimum in terms of thickness and chemical composition (for bonding with rubber) at 140 °C, and a further increase in VT results in thicker and larger crystalline nanostructures, resulting in a weak interfacial strength with rubber.[12,13] It can therefore be concluded that 140 °C serves as the optimum VT in the present case as the interfacial thickness and its composition were proper for better bonding with rubber.

Figures 5A1 to 5E1 represent high-resolution TEM images of the hexagonal nanostructures formed at the interface. It is quite evident from Figures 5A1 to 5E1 that a heterojunction having different compositions (i.e., multiphase system) was

https://dx.doi.org/10.1021/acsanm.0c01298
ACS Appl. Nano Mater. 2020, 3, 7685−7694

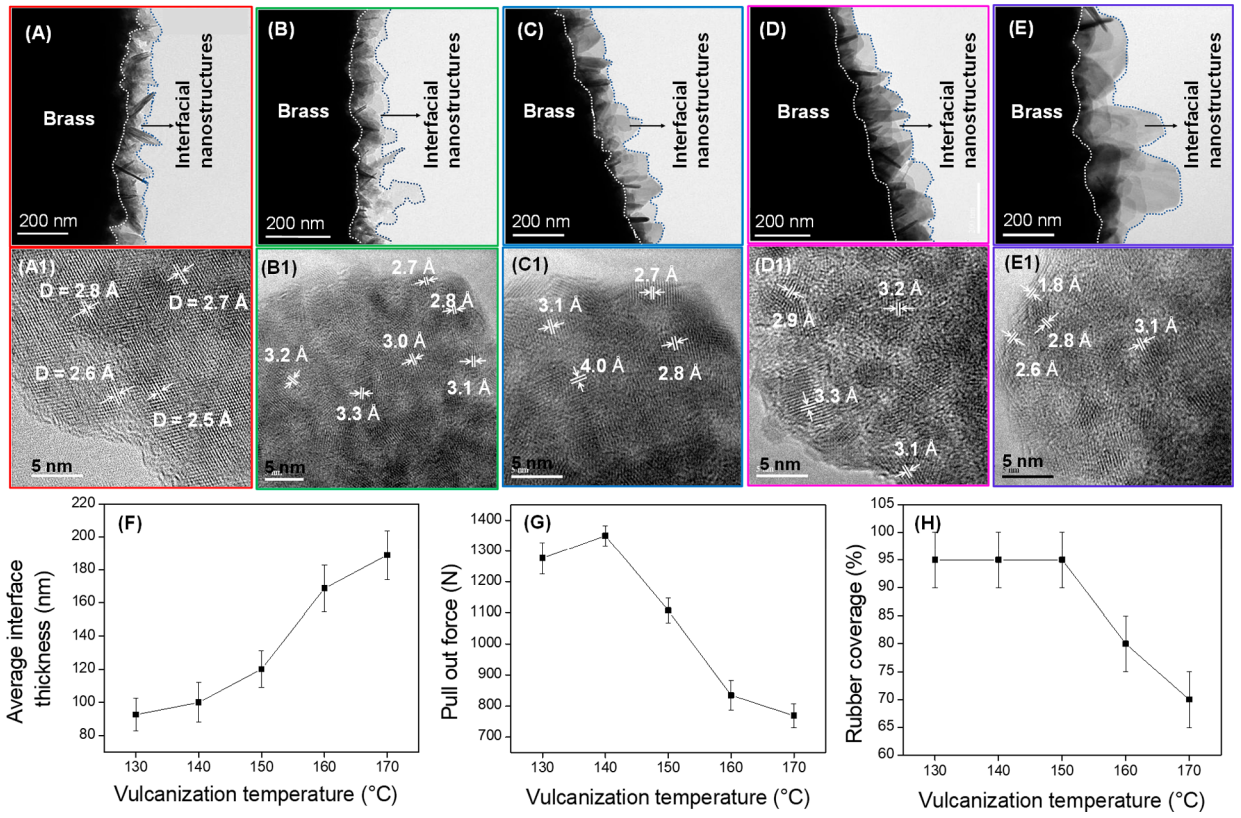

Figure 5. Bright-field TEM images of the hexagonal nanoplates grown over brass mesh vulcanized at (A) 130, (B) 140, (C) 150, (D) 160, and (E) 170 °C. Corresponding HRTEM images are in (A1)−(E1). Scale bar: 5 nm. Various lattice dimensions seen are marked. Graphical representation of (F) the average interface thickness, (G) variation in POF, and (H) rubber coverage as a function of vulcanization temperature.

formed. After vulcanization, rubber is in immediate contact with these phases, and the presence of each phase marks its importance at the interface. The lattice spacings at 130 °C corresponded to the presence of (103) planes of CuS, (018) planes of ZnS, and (301) and (221) planes of $Cu_{1.75}S$, which are in line with the XRD patterns (Figure 4).[42,43] The topmost layer of nanostructures that are in contact with rubber was composed of a triphase composition (having four lattice fringes) of CuS, $Cu_{1.75}S$, and ZnS. At 140 °C, the lattice structure is comprised of the (013) plane of CuS, the (111) plane of $Cu_{1.8}S$, and the (014) and (015) planes of ZnS, which was more or less the same until 160 °C.[44] The lattice spacing at 170 °C corresponded to the presence of the (013) plane of CuS, the (111) plane of Cu_2S, and the (011) plane of ZnO.[45]

Through the TEM experiments using the brass mesh, we have presented a simple technique to measure the thickness of the brass−rubber interface and its chemical composition and have correlated the interface thickness with POF measurements.

3.4. Understanding the Chemical State at the Brass−Rubber Interface. XPS analysis was performed on the vulcanized steel cords to find the chemical composition and oxidation states of the elements formed at the interface. Generally, in copper chalcogenides, the valence band is formed from the p orbital while the conduction band is constructed from 4s and 4p orbitals of Cu.[46] In the case of stoichiometric Cu_2S, the valence band is filled up. On the contrary, the structure of CuS is distinct from that of Cu_2S. CuS has a repeating layer of CuS_3 that is sandwiched between CuS_4 tetrahedra, and this triple layer is connected to other triple layers through disulfide bonds. The valency of Cu in CuS is found to be between 1 and 1.5, and recent calculations suggest the valency of Cu to be 1.33.[47,48] When nonstoichiometry occurs during vulcanization, Cu vacancies are created in the lattice which affects the valency of the cation. In addition to CuS and Cu_2S, other types of $Cu_{2-x}S$ are also formed in the adhesion interface, but distinguishing them by using XPS is challenging. To cite an example, the difference in binding energy (BE) between Cu_2S and $Cu_{1.75}S$ is just 0.2 eV.

The different chemical species formed at the interface are reflected from the change in peak binding energy values of XPS. Figure S7 indicates that the unvulcanized brass surface had a higher peak intensity of Zn than of Cu, proving that ZnO was present on the surface before vulcanization. The C 1s peaks originated from either the tiny amount of filter paper sticking on the surface or as a result of adventitious C, while O 1s was identified to be from the metal oxides. Figure 6 shows the peak fitting analysis of S 2p, Cu $2p_{3/2}$ and $2p_{1/2}$, Zn $2p_{3/2}$ regions. Cu- and S-related peaks started to increase during vulcanization as a result of the formation of copper sulfides. Vulcanization of the BCSC from 130 to 160 °C gave rise to CuS (BE = 932.2 eV) and ZnS (BE = 1021.8 eV) at the interface. Even though $Cu_{1.75}S$ and $Cu_{1.8}S$ were formed between 130 and 160 °C (as found by XRD and TEM), no separate peaks for them were observed in XPS. We note that the difference in binding energy between CuS and $Cu_{2-x}S$ is very narrow. At 170 °C, the interface mostly consists of Cu_2S (BE = 932.8 eV) and ZnO (BE = 1022.5 eV).[32] More information about the chemical state of the interface was obtained from the S 2p core-level XPS data. The $2p_{3/2}/2p_{1/2}$ doublet of S was filled with a ΔJ of 1.18 eV. Vulcanization at 130−160 °C resulted in S $2p_{3/2}$ at 161.2 eV, confirming the

https://dx.doi.org/10.1021/acsanm.0c01298
ACS Appl. Nano Mater. 2020, 3, 7685−7694

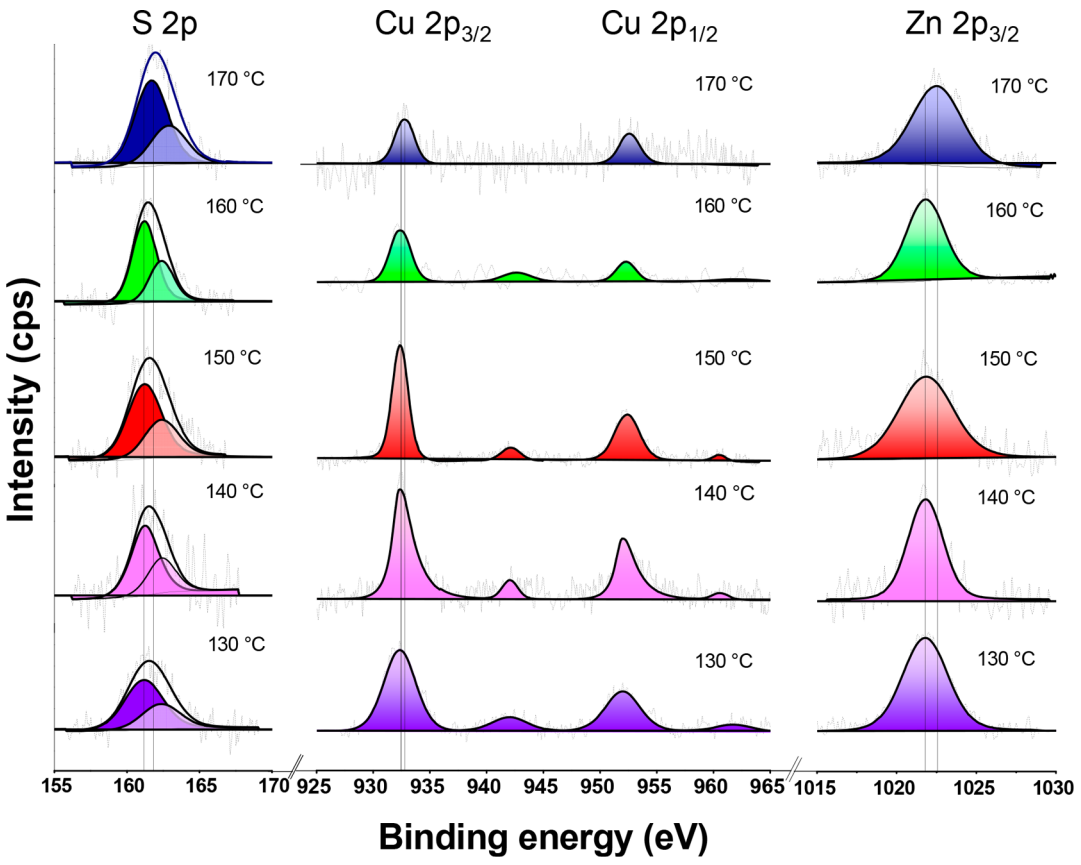

Figure 6. High-resolution XPS spectra of S 2p, Cu $2p_{3/2}$, Cu $2p_{1/2}$, and Zn $2p_{3/2}$ formed during vulcanization of BCSC from 130 to 170 °C. The dark lines in the spectra depict peak fitting.

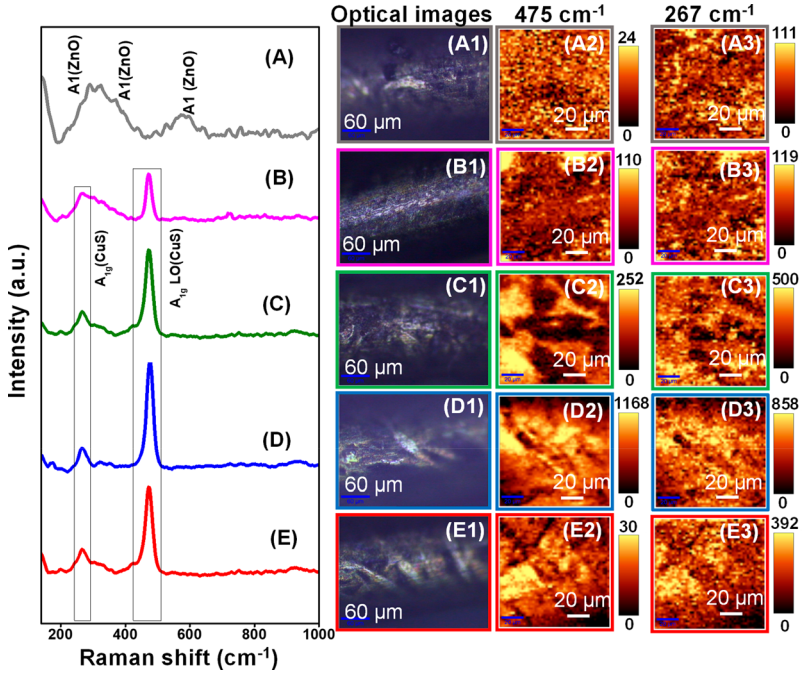

Figure 7. Raman spectra of BCSC at (A) 170, (B) 160, (C) 150, (D) 140, and (E) 130 °C. Images (A1) to (E1) represent Raman optical images (scale: 60 μm), images (A2) to (E2) correspond to confocal Raman maps of CuS at 475 cm^{-1} (scale: 20 μm), and images (A3) to (E3) correspond to confocal Raman maps of CuS at 267 cm^{-1} (scale: 20 μm). The color bars on the extreme right indicate the CCD counts.

presence of CuS. At 170 °C, the emergence of S $2p_{3/2}$ at 161.7 eV was seen due to Cu_2S.

The amount of Cu, Zn, O, and S present at the interface during vulcanization is a measure of interfacial adhesion. The atomic percent (at. %) found by XPS showed that Cu and S

https://dx.doi.org/10.1021/acsanm.0c01298
ACS Appl. Nano Mater. 2020, 3, 7685−7694

kept increasing from 130 to 170 °C in vulcanized BCSC (Figure S8). This indicates an increase in copper sulfide formation with increase in VT. Increase of Cu at. % correlated directly to a reduction in POF at higher VTs. The at. % of Zn and O increases up to 170 °C VT, indicating the formation of ZnO. Higher Cu at. % indicated that the interface thickness increased with VT, and a thicker interface is prone to break easily under the application of stress.

Understanding CuS Concentration Distribution throughout the Brass−Rubber Interface Using Confocal Raman Spectroscopy and Microscopy. Raman spectroscopy coupled with imaging is a powerful technique that provides detailed chemical information about the interface. Figures S9A and S9B represent the optical image and Raman spectra of the unreacted BCSC. Raman spectra of unreacted BCSC suggested the presence of CuO along with ZnO on the surface of brass. Raman spectra of the BCSC after vulcanization are shown in Figures 7A−E, representing a change in the chemical nature of brass, post-vulcanization (130−170 °C). The interface was investigated pixel by pixel through the Raman map to generate false-color images (Raman mapping) based on the interfacial chemical composition. Figures 7A1 to 7E1 depict the optical images, and Figures 7A2 to 7E2 show the confocal Raman maps at 475 cm^{-1}; Figures 7A3 to 7E3 are due to the feature at 267 cm^{-1}.

Sharp peaks were observed at 475 and 267 cm^{-1} between 130 and 160 °C. The former peak corresponded to A_{1g} LO of CuS while the latter corresponded to A_{1g} peak of CuS.[32,42] It can be noted that the peak intensities were stronger at 130, 140, and 150 °C and have comparatively reduced in intensity at 160 °C. Distinguishing a mixture of $Cu_{1.75}S$ and $Cu_{1.8}S$ in CuS from the Raman spectrum is challenging, as both $Cu_{1.75}S$ and $Cu_{1.8}S$ show a prominent peak at 469 cm^{-1}. However, Raman peaks corresponding to ZnS get submerged as the intensities of CuS (475 and 274 cm^{-1}) were multifold more than ZnS. Characteristic peaks at 574, 437, 407, and 380 cm^{-1} corresponded to the presence of ZnO at 170 °C. XRD and XPS results support the formation of $Cu_{1.95}S$ and Cu_2S along with ZnO at 170 °C, but no peak for Cu_2S is seen in Figures 7A−E, as it is a Raman-inactive molecule.

Raman mapping using the peaks at 475 and 267 cm^{-1} showed that CuS is more prominent in the adhesion interface. Bright regions were observed in the generated heat maps shown in Figures 7A2 to 7E3. The gradual increase in the black regions from 130 to 170 °C indicates regions in the steel cord that are having lesser concentration of CuS. From these data, we believe that Raman mapping can be used as a tool to understand the concentration distribution of CuS at the brass−rubber interface as a function of VT.

CONCLUSION

We developed a methodology, the "brass-mesh experiment", for measuring the growth of nanostructures formed at the interface between rubber and brass as a function of vulcanization temperature (VT, 130−170 °C). The interfacial nanostructures grow in size (thickness) from ∼90 to ∼190 nm as the VT was increased from 130 to 170 °C. Scanning electron microscopy (SEM) shows that the morphology of the nanostructures varies from flaky type to nanopillar-like with increase in VT. The brass-mesh TEM study shows that the nanostructures grow in size, and the lattice-resolved TEM images indicated the formation of CuS, $Cu_{1.75}S$, $Cu_{1.8}S$, ZnS, and ZnO under the vulcanization conditions. This was additionally confirmed by X-ray diffraction (XRD) and X-ray photoelectron spectroscopy (XPS) investigations. Raman spectroscopy and imaging are used for the first time in the literature to map the spatial distribution of the sulfides and oxides formed. Using the above methodology, we could optimize the vulcanization temperature to 140 °C for the mentioned rubber composition. We believe that the results presented in this paper will be immensely useful to the tire and allied rubber industries and will trigger further research in this area as the interfacial adhesion is crucial to the durability of radial tires and safety of passengers.

ASSOCIATED CONTENT

Supporting Information

The Supporting Information is available free of charge at https://pubs.acs.org/doi/10.1021/acsanm.0c01298.

Schematic image of laser cut mesh from brass foil that is used for interfacial thickness experiment; schematic showing pull-out force measurement procedure; microscopic images of reacted brass-coated steel cords with change in vulcanization temperature; SEM-EDS data of vulcanized cords; physical properties of rubber compound with increasing vulcanization temperature; XRD pattern of unvulcanized brass-coated steel cord; XPS survey spectra of unreacted brass-coated steel cord under ambient conditions; relative at. % obtained from XPS; Raman spectra and LED white light image of unreacted BCSC; total cross-link density of rubber compound at different vulcanization temperatures (PDF)

AUTHOR INFORMATION

Corresponding Authors

A. Sreekumaran Nair − *R&D Centre, MRF Limited, Chennai 600019, India;* orcid.org/0000-0001-9258-8566; Email: sreekumaran.nair@mrfmail.com

Thalappil Pradeep − *DST Unit of Nanoscience (DST UNS) and Thematic Unit of Excellence (TUE), Department of Chemistry, Indian Institute of Technology Madras, Chennai 600036, India;* orcid.org/0000-0003-3174-534X; Email: pradeep@iitm.ac.in

Authors

M. P. Kannan − *DST Unit of Nanoscience (DST UNS) and Thematic Unit of Excellence (TUE), Department of Chemistry, Indian Institute of Technology Madras, Chennai 600036, India; R&D Centre, MRF Limited, Chennai 600019, India;* orcid.org/0000-0001-5526-2620

Anirban Som − *DST Unit of Nanoscience (DST UNS) and Thematic Unit of Excellence (TUE), Department of Chemistry, Indian Institute of Technology Madras, Chennai 600036, India;* orcid.org/0000-0002-6646-679X

Tripti Ahuja − *DST Unit of Nanoscience (DST UNS) and Thematic Unit of Excellence (TUE), Department of Chemistry, Indian Institute of Technology Madras, Chennai 600036, India;* orcid.org/0000-0002-9256-2689

Vidhya Subramanian − *DST Unit of Nanoscience (DST UNS) and Thematic Unit of Excellence (TUE), Department of Chemistry, Indian Institute of Technology Madras, Chennai 600036, India;* orcid.org/0000-0002-6076-3515

Complete contact information is available at: https://pubs.acs.org/10.1021/acsanm.0c01298

https://dx.doi.org/10.1021/acsanm.0c01298
ACS Appl. Nano Mater. 2020, 3, 7685−7694

Funding

This work was financially supported by MRF Ltd. through a research grant. Equipment used in this work was supported by the Department of Science and Technology.

Notes

The authors declare no competing financial interest.

■ ACKNOWLEDGMENTS

The authors thank Prof. G. U. Kulkarani, Jawaharlal Nehru Centre for Advanced Scientific Research (JNCASR), for FESEM measurements. T.P. thanks MRF Ltd. for a research grant. The authors thank the Department of Science and Technology, Government of India, for equipment support through the Nano Mission.

■ REFERENCES

(1) Kane, K.; Jumel, J.; Lallet, F.; Mbiakop Ngassa, A.; Vacherand, J. M.; Shanahan, M. E. R. A novel inflation adhesion test for elastomeric matrix/steel cord. *Int. J. Solids Struct.* **2019**, *160*, 40−50.

(2) Ogawa, H.; Furuya, S.; Koseki, H.; Iida, H.; Sato, K.; Yamagishi, K. A Study on the Contour of the Truck and Bus Radial Tire. *Tire Sci. Technol.* **1990**, *18* (4), 236−261.

(3) Dhanalakshmi, J.; Vijayakumar, C. T. Thermal studies on dry bonding adhesive system for potential rubber article applications. *J. Adhes. Sci. Technol.* **2020**, *34* (3), 233−245.

(4) Han, Y. H.; Becker, E. B.; Fahrenthold, E. P.; Kim, D. M. Fatigue Life Prediction for Cord-Rubber Composite Tires Using a Global-Local Finite Element Method. *Tire Sci. Technol.* **2004**, *32* (1), 23−40.

(5) Park, C. H.; Lee, W. I.; Yoo, Y. E.; Kim, E. G. A study on fiber orientation in the compression molding of fiber reinforced polymer composite material. *J. Mater. Process. Technol.* **2001**, *111* (1), 233−239.

(6) Hamed, G. R.; Huang, J. Combining Cobalt and Resorcinolic Bonding Agents in Brass-Rubber Adhesion. *Rubber Chem. Technol.* **1991**, *64* (2), 285−295.

(7) Maghsoudi, K.; Momen, G.; Jafari, R.; Farzaneh, M. Direct replication of micro-nanostructures in the fabrication of super-hydrophobic silicone rubber surfaces by compression molding. *Appl. Surf. Sci.* **2018**, *458*, 619−628.

(8) Van Ooij, W. J. Mechanism and Theories of Rubber Adhesion to Steel Tire Cords—An Overview. *Rubber Chem. Technol.* **1984**, *57* (3), 421−456.

(9) Buytaert, G.; Coornaert, F.; Dekeyser, W. Characterization of the Steel Tire Cord - Rubber Interface. *Rubber Chem. Technol.* **2009**, *82* (4), 430−441.

(10) Pekachaki, H. M.; Taghvaei-Ganjali, S.; Motiee, F.; Saber-Tehrani, M. Application of Calixarene Derivatives as Tackifier Resin in Rubber Compounds for Tire Applications. *Rubber Chem. Technol.* **2019**, *92* (3), 467−480.

(11) Vandenabeele, C.; Bulou, S.; Maurau, R.; Siffer, F.; Belmonte, T.; Choquet, P. Organo-Chlorinated Thin Films Deposited by Atmospheric Pressure Plasma-Enhanced Chemical Vapor Deposition for Adhesion Enhancement between Rubber and Zinc-Plated Steel Monofilaments. *ACS Appl. Mater. Interfaces* **2015**, *7* (26), 14317−14327.

(12) Van Ooij, W. J.; Harakuni, P. B.; Buytaert, G. Adhesion of Steel Tire Cord to Rubber. *Rubber Chem. Technol.* **2009**, *82* (3), 315−339.

(13) Fulton, W. S. Steel Tire Cord-Rubber Adhesion, Including the Contribution of Cobalt. *Rubber Chem. Technol.* **2005**, *78* (3), 426−457.

(14) Sarlin, E.; Rosling, A.; Honkanen, M.; Lindgren, M.; Juutilainen, M.; Poikelispää, M.; Laihonen, P.; Vippola, M.; Vuorinen, J. Effect of Environment on Bromobutyl Rubber-Steel Adhesion. *Rubber Chem. Technol.* **2020**, *93*, 429−444.

(15) Jeon, G. S.; Seo, G. Influence of Cure Conditions on the Adhesion of Rubber Compound to Brass-plated Steel Cord. Part I. Cure Temperature. *J. Adhes.* **2001**, *76* (3), 201−221.

(16) Ozawa, K.; Kakubo, T.; Amino, N.; Mase, K.; Ikenaga, E.; Nakamura, T. Angle-Resolved HAXPES Investigation on the Chemical Origin of Adhesion between Natural Rubber and Brass. *Langmuir* **2017**, *33* (38), 9582−9589.

(17) Ling, C. Y.; Hirvi, J. T.; Suvanto, M.; Bazhenov, A. S.; Markkula, K.; Hillman, L.; Pakkanen, T. A. Effect of cobalt additives and mixed metal sulfides at rubber−brass interface on rubber adhesion: a computational study. *Theor. Chem. Acc.* **2017**, *136* (2), 24.

(18) Chen, Y.; Schlarb, J. L. Steel Cord−Rubber Adhesion with SEM/EDX. *Tire Sci. Technol.* **2018**, *46* (1), 27−37.

(19) Ozawa, K.; Kakubo, T.; Shimizu, K.; Amino, N.; Mase, K.; Komatsu, T. High-resolution photoelectron spectroscopy analysis of sulfidation of brass at the rubber/brass interface. *Appl. Surf. Sci.* **2013**, *264*, 297−304.

(20) Fulton, W. S.; Sykes, D. E.; Smith, G. C. SIMS depth profiling of rubber-tyre cord bonding layers prepared using 64Zn depleted ZnO. *Appl. Surf. Sci.* **2006**, *252* (19), 7074−7077.

(21) Patil, P. Y.; Van Ooij, W. J. Mechanism of Improved Aged Rubber-to-Brass Adhesion Using One-Component Resins. *Rubber Chem. Technol.* **2005**, *78* (1), 155−173.

(22) Kim, J. M.; van Ooij, W. J. Study of the effects of compounding ingredients on the adhesion layer between squalene model compound and brass by GPC and TOF-SIMS. *J. Adhes. Sci. Technol.* **2003**, *17* (2), 165−178.

(23) Shimizu, K.; Miyata, T.; Nagao, T.; Kumagai, A.; Jinnai, H. Visualization of the tensile fracture behaviors at adhesive interfaces between brass and sulfur-containing rubber studied by transmission electron microscopy. *Polymer* **2019**, *181*, 121789.

(24) Kakubo, T.; Shimizu, K.; Kumagai, A.; Matsumoto, H.; Tsuchiya, M.; Amino, N.; Jinnai, H. Degradation of a Metal−Polymer Interface Observed by Element-Specific Focused Ion Beam-Scanning Electron Microscopy. *Langmuir* **2020**, *36* (11), 2816−2822.

(25) Jeon, G. S. On characterizing microscopically the adhesion interphase for the adhesion between metal and rubber compound Part III. Effect of brass-plating amount for brass-plated steel cord. *J. Adhes. Sci. Technol.* **2017**, *31* (24), 2667−2681.

(26) Ozawa, K.; Mase, K. Evidence for chemical bond formation at rubber-brass interface: Photoelectron spectroscopy study of bonding interaction between copper sulfide and model molecules of natural rubber. *Surf. Sci.* **2016**, *654*, 14−19.

(27) Ozawa, K.; Kakubo, T.; Shimizu, K.; Amino, N.; Mase, K.; Ikenaga, E.; Nakamura, T.; Kinoshita, T.; Oji, H. In situ chemical state analysis of buried polymer/metal adhesive interface by hard X-ray photoelectron spectroscopy. *Appl. Surf. Sci.* **2014**, *320*, 177−182.

(28) Jeon, G. S.; Seo, G. Influence of Cure Conditions on the Adhesion of Rubber Compound to Brass-plated Steel Cord. Part II. Cure Time. *J. Adhes.* **2001**, *76* (3), 223−244.

(29) Hotaka, T.; Ishikawa, Y.; Mori, K. Characterization of Adhesion Interlayer Between Rubber and Brass by a Novel Method of Sample Preparation. *Rubber Chem. Technol.* **2007**, *80* (1), 61−82.

(30) Ziegler, E.; Macher, J.; Gruber, D.; Pölt, P.; Kern, W.; Lummerstorfer, T.; Feldgitscher, C.; Holzner, A.; Trimmel, G. Investigation of the Influence of Stearic Acid on Rubber-Brass Adhesion. *Rubber Chem. Technol.* **2012**, *85* (2), 264−276.

(31) Van Ooij, W. J. The Role of XPS in the Study and Understanding of Rubber-to-Metal Bonding. *Surf. Sci.* **1977**, *68*, 1−9.

(32) Baert, K.; Breugelmans, T.; Buytaert, G.; Brabant, J. V.; Hubin, A. The combination of surface enhanced Raman spectroscopy and an ionic liquid as a model system to study the adhesion interface between sulfur and brass. *J. Raman Spectrosc.* **2013**, *44* (3), 377−381.

(33) Seo, G. Stabilizing the adhesion interphase between rubber compounds and brass film by the addition of resorcinol formaldehyde resin to the rubber. *J. Adhes. Sci. Technol.* **1997**, *11* (11), 1433−1445.

(34) Mukhopadhyay, R.; Sadhan, K. D.; Chakraborty, S. N. Effect of Vulcanization Temperature and Vulcanization Systems on The Structure and Properties of Natural Rubber Vulcanizates. *Polymer* **1977**, *18* (12), 1243−1249.

https://dx.doi.org/10.1021/acsanm.0c01298
ACS Appl. Nano Mater. 2020, 3, 7685−7694

(35) Debasish, D.; Debapriya, D.; Adhikari, B. The effect of grass fiber filler on curing characteristics and mechanical properties of natural rubber. *Polym. Adv. Technol.* **2004**, *15* (12), 708−715.
(36) Ghosh, P.; Katare, S.; Patkar, P.; Caruthers, J. M.; Venkatasubramanian, V.; Walker, K. A. Sulfur Vulcanization of Natural Rubber for Benzothiazole Accelerated Formulations: From Reaction Mechanisms to a Rational Kinetic Model. *Rubber Chem. Technol.* **2003**, *76* (3), 592−693.
(37) Luther, J. M.; Jain, P. K.; Ewers, T.; Alivisatos, A. P. Localized surface plasmon resonances arising from free carriers in doped quantum dots. *Nat. Mater.* **2011**, *10* (5), 361−366.
(38) Li, W.; Zamani, R.; Rivera Gil, P.; Pelaz, B.; Ibanez, M.; Cadavid, D.; Shavel, A.; Alvarez-Puebla, R. A.; Parak, W. J.; Arbiol, J.; Cabot, A. CuTe Nanocrystals: Shape and Size Control, Plasmonic Properties, and Use as SERS Probes and Photothermal Agents. *J. Am. Chem. Soc.* **2013**, *135* (19), 7098−7101.
(39) Li, W.; Zamani, R.; Ibanez, M.; Cadavid, D.; Shavel, A.; Morante, J. R.; Arbiol, J.; Cabot, A. Metal Ions To Control the Morphology of Semiconductor Nanoparticles: Copper Selenide Nanocubes. *J. Am. Chem. Soc.* **2013**, *135* (12), 4664−4667.
(40) Hotaka, T.; Ishikawa, Y.; Mori, K. Effect of Compound Ingredients on Adhesion between Rubber and Brass-Plated Steel Cord. *Rubber Chem. Technol.* **2005**, *78* (2), 175−187.
(41) Chandra, A. K.; Mukhopadhyay, R.; Konar, J.; Ghosh, T. B.; Bhowmick, A. K. X-ray photoelectron spectroscopy and Auger electron spectroscopy of the influence of cations and anions of organometallic adhesion promoters on the interface between steel cord and rubber skim compounds. *J. Mater. Sci.* **1996**, *31* (10), 2667−2676.
(42) Shawky, A.; El-Sheikh, S. M.; Gaber, A.; El-Hout, S. I.; El-Sherbiny, I. M.; Ahmed, A. I. Urchin-like CuS nanostructures: simple synthesis and structural optimization with enhanced photocatalytic activity under direct sunlight. *Appl. Nanosci.* **2020**, *10*, 2153−2164.
(43) Pattrick, R. A. D.; Mosselmans, J. F. W.; Charnock, J. M.; England, K. E. R.; Helz, G. R.; Garner, C. D.; Vaughan, D. J. The structure of amorphous copper sulfide precipitates: An X-ray absorption study. *Geochim. Cosmochim. Acta* **1997**, *61* (10), 2023−2036.
(44) Park, H.; Kwon, J.; Kim, J.; Park, K.; Song, T.; Paik, U. Facile Growth of Metal-Rich $Cu_{1.75}S$ and $Cu_{1.8}S$ Microspheres Assembled with Mesoporous Nanosheets and Their Application in Na-Ion Batteries. *Cryst. Growth Des.* **2020**, *20*, 3325−3333.
(45) Peng, M.; Ma, L.-L.; Zhang, Y.-G.; Tan, M.; Wang, J.-B.; Yu, Y. Controllable synthesis of self-assembled Cu2S nanostructures through a template-free polyol process for the degradation of organic pollutant under visible light. *Mater. Res. Bull.* **2009**, *44* (9), 1834−1841.
(46) Garba, E. J. D.; Jacobs, R. L. The electronic structure of $Cu_{2-x}Se$. *Physica B+C* **1986**, *138* (3), 253−260.
(47) Liang, W.; Whangbo, M. H. Conductivity anisotropy and structural phase transition in Covellite CuS. *Solid State Commun.* **1993**, *85* (5), 405−408.
(48) Mazin, I. I. Structural and electronic properties of the two-dimensional superconductor CuS with 1 1/3-valent copper. *Phys. Rev. B: Condens. Matter Mater. Phys.* **2012**, *85* (11), 115−133.

https://dx.doi.org/10.1021/acsanm.0c01298
ACS Appl. Nano Mater. 2020, 3, 7685−7694